RADIATION RESEARCH **184**, 322–333 (2015)
0033-7587/15 $15.00

DOI: 10.1667/RR13919.1

Treating Brain Tumor with Microbeam Radiation Generated by a Compact Carbon-Nanotube-Based Irradiator: Initial Radiation Efficacy Study

Hong Yuan,[a,b,1] Lei Zhang,[c] Jonathan E. Frank,[b] Christina R. Inscoe,[c,d] Laurel M. Burk,[d,2] Mike Hadsell,[d,3] Yueh Z. Lee,[a,b,d,e,g] Jianping Lu,[c,d] Sha Chang[d,e,f,g] and Otto Zhou[c,d,g]

[a] *Department of Radiology,* [b] *Biomedical Imaging Research Center,* [c] *Department of Applied Physical Sciences,* [d] *Department of Physics and Astronomy,* [e] *Department of Biomedical Engineering,* [f] *Department of Radiation Oncology and* [g] *Lineberger Comprehensive Cancer Center, University of North Carolina at Chapel Hill, Chapel Hill, North Carolina 27599*

Yuan, H., Zhang, L., Frank, J., Inscoe, C. I., Burk, L. M., Hadsell, M., Lee, Y., Lu, J., Chang, S. and Zhou, O. Treating Brain Tumor with Microbeam Radiation Generated by a Compact Carbon-Nanotube-Based Irradiator: Initial Radiation Efficacy Study. *Radiat. Res.* 184, 322–333 (2015).

Microbeam radiation treatment (MRT) using synchrotron radiation has shown great promise in the treatment of brain tumors, with a demonstrated ability to eradicate the tumor while sparing normal tissue in small animal models. With the goal of expediting the advancement of MRT research beyond the limited number of synchrotron facilities in the world, we recently developed a compact laboratory-scale microbeam irradiator using carbon nanotube (CNT) field emission-based X-ray source array technology. The focus of this study is to evaluate the effects of the microbeam radiation generated by this compact irradiator in terms of tumor control and normal tissue damage in a mouse brain tumor model. Mice with U87MG human glioblastoma were treated with sham irradiation, low-dose MRT, high-dose MRT or 10 Gy broad-beam radiation treatment (BRT). The microbeams were 280 μm wide and spaced at 900 μm center-to-center with peak dose at either 48 Gy (low-dose MRT) or 72 Gy (high-dose MRT). Survival studies showed that the mice treated with both MRT protocols had a significantly extended life span compared to the untreated control group (31.4 and 48.5% of life extension for low- and high-dose MRT, respectively) and had similar survival to the BRT group. Immunostaining on MRT mice demonstrated much higher DNA damage and apoptosis level in tumor tissue compared to the normal brain tissue. Apoptosis in normal tissue was significantly lower in the low-dose MRT group compared to that in the BRT group at 48 h postirradiation. Interestingly, there was a significantly higher level of cell proliferation in the MRT-treated normal tissue compared to that in the BRT-treated mice, indicating rapid normal tissue repairing process after MRT. Microbeam radiation exposure on normal brain tissue causes little apoptosis and no macrophage infiltration at 30 days after exposure. This study is the first biological assessment on MRT effects using the compact CNT-based irradiator. It provides an alternative technology that can enable widespread MRT research on mechanistic studies using a preclinical model, as well as further translational research towards clinical applications.

INTRODUCTION

Despite recent developments in the treatment of glioblastoma multiforme (GBM) the median survival for glioblastoma is still limited to 12 months on average (*1, 2*). While radiation therapy is one of the primary treatments for brain tumors, effective brain tumor control is often limited by the risk of collateral radiation-induced damage to the surrounding normal brain tissue (*3, 4*). Therefore, reducing normal tissue toxicity while enhancing tumor control, and improving the overall therapeutic efficacy, remains a goal in radiation therapy.

Microbeam radiation treatment (MRT) is a unique form of spatially fractioned radiation therapy that uses parallel thin planar X-ray beams for treatment. In many preclinical studies, MRT has demonstrated effective tumor cell killing, while sparing normal tissue (*5–11*). However, given the small number of synchrotron radiation facilities around the world that are available to provide MRT, advances in MRT and potential clinical translation are greatly hindered. To promote widespread MRT research in the scientific community, our group recently developed a compact X-ray microbeam irradiator based on carbon nanotube (CNT) field emission technology (*12, 13*). The compact system is not designed to reproduce the exact radiation profile and dosimetry generated by the large synchrotron-based MRT facilities, but to investigate the microbeam radiation dosimetry required to produce similar MRT radiobiological

Editor's note. The online version of this article (DOI: 10.1667/RR13919.1) contains supplementary information that is available to all authorized users.

[1] Address for correspondence: 130 Mason Farm Road, CB no. 7513, UNC Chapel Hill, Chapel Hill, NC 27599; e-mail: yuanh@med.unc.edu.

[2] Current address: U.S. Food and Drug Administration, Silver Spring, MD.

[3] Current address: Department of Radiation Oncology, Stanford University School of Medicine, Stanford, CA.

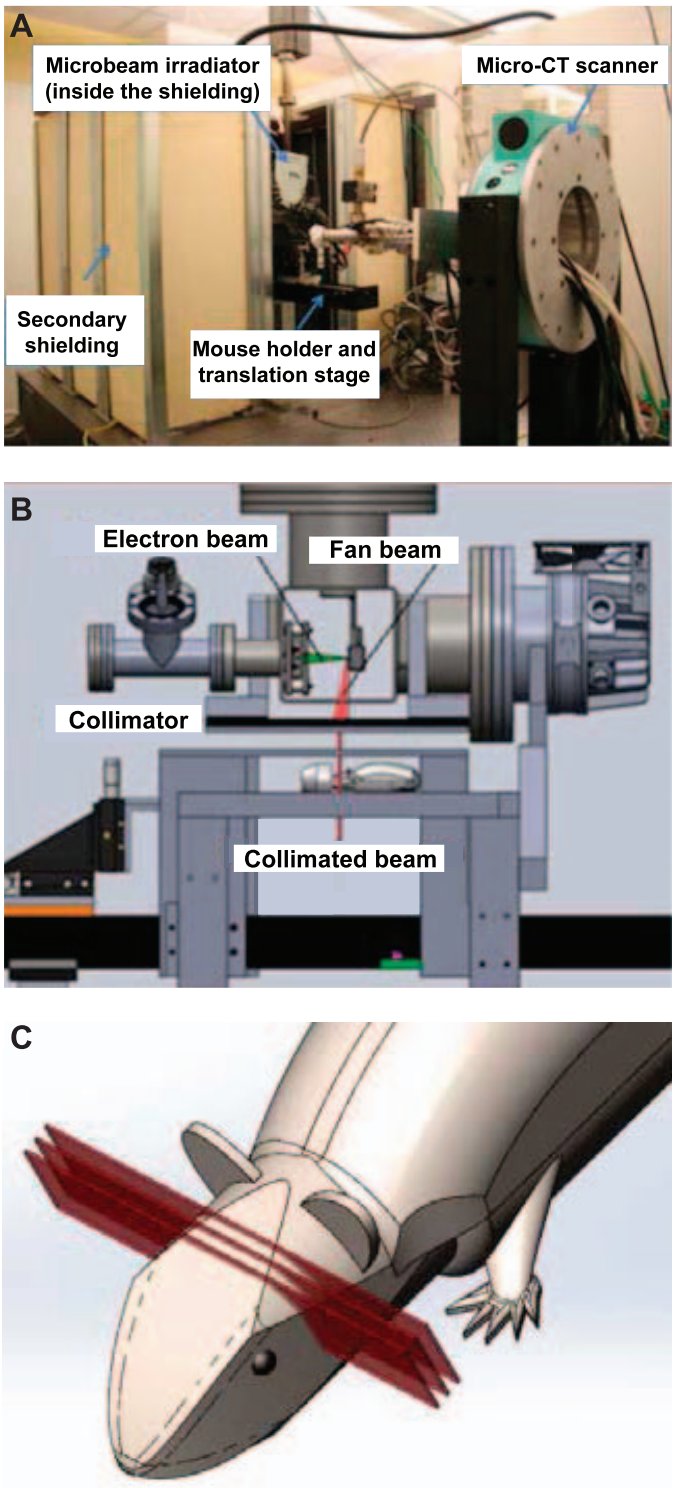

FIG. 1. System structure and components of the compact carbon-nanotube-based (CNT) microbeam irradiator. Panel A: MicroCT integrated microbeam irradiator setup in the laboratory. Panel B: Structure diagram of the microbeam irradiator. Panel C: Cartoon diagram demonstrating three arrays of planar microbeams applied on mouse head for treatment [modified and used with permission, Zhang *et al*. Phys Med Biol 2014; 59:1283–303 (*16*)].

outcomes. The first preclinical prototype we developed (Fig. 1) contains a CNT field emission cathode array and a tungsten anode with a long and narrow focal line to produce optimally distributed X-ray microbeam with adjustable beam width (*14*). The distributed CNT X-ray source design maximizes microbeam dose rate by spreading the total thermal power to a long focal track (0.142×160 mm), and this cannot be achieved by the small focal point design used in most conventional X-ray tubes. Our compact microbeam system is different from the synchrotron irradiation system, since it electronically controls the radiation and thus allows real-time gated radiation delivery using respiratory or cardiac signals to accurately deliver the radiation under organ motions (*15*). An image-guided MRT protocol has been established for mouse brain tumor treatment, where magnetic resonance images were registered to the on-board X-ray radiography images of mouse brain to guide the delivery of microbeam radiation to the brain tumor with an average 450 μm accuracy (*16*). The current study used the same image-guided MRT protocol reported earlier, and aimed to evaluate radiobiological effects from MRT.

In this radiobiologically focused study, we evaluated the effects of MRT on both brain tumor and normal brain tissue in a U87MG human glioblastoma-bearing mouse model using this compact CNT-based microbeam irradiator. Survival studies were conducted and tumor volume was monitored using MRI after radiation treatment. Immunostaining of γ-H2AX, caspase-3, Ki-67 and F4/80 proteins was performed at different time points after MRT to assess radiation-induced DNA double-strand breaks (DSBs), apoptosis, cell proliferation and neuroinflammation, respectively. MRT effects on normal mice without tumor were also evaluated at acute (24 h) and delayed (day 30) phases after MRT. This study is the first to characterize the MRT effects on brain tumor and normal tissue using the compact CNT-based image-guided MRT system.

MATERIALS AND METHODS

Brain Tumor Mouse Model

Male athymic nude mice (4–6 weeks old) were used for brain tumor inoculation. U87MG human glioblastoma tumor cells were obtained from Dr. C. Ryan Miller, University of North Carolina (UNC; Chapel Hill, NC) and maintained in our laboratory. About 2×10^5 cells in 5 μl culture media mixed with 5% methylcellulose were injected into the forebrain of mice using the stereotaxic technique at 1 mm anterior, 2 mm lateral to the bregma and 4 mm deep from the surface to form the orthotopic xenograft glioblastoma mouse model. Three weeks after tumor cell injection, the mice were brought to the Imaging Core Facility for MRI and subsequent radiation treatment. All animal handling and experimental procedures in the study were approved by the Institutional Animal Care and Use Committee at University of North Carolina.

Magnetic Resonance Imaging

Mouse brain MRIs were performed on a small animal 9.4 Tesla MRI system (Bruker Inc., Billerica, MA) at the UNC Small Animal Imaging Core Facility. T2-weighted images were acquired using a rapid acquisition with refocused echoes (RARE) sequence with the

following parameters: TE/TR = 22/3,400 ms, 256 × 256 matrix size, 0.5 mm slice thickness and 100 μm in-plane resolutions. Tumor volume was measured by manually demarcating the tumor region on each MRI slice using ImageJ (version 1.46r, imagej.nih.gov/ij; ImageJ Software, National Institutes of Health, Bethesda, MD). Mice were initially imaged at 3 weeks after tumor cell inoculation for tumor localization and volume measurement. After irradiation, mice were imaged using the same MRI protocol weekly for two weeks after MRT to monitor changes in tumor volume.

Microbeam Radiation Treatment

Microbeam irradiation to the mouse brain was performed using the prototype compact CNT-based MRT system. Figure 1 shows the system diagram and an illustration of radiation beam delivery to the mouse head. The microbeam irradiator runs at a constant anode voltage of 160 kVp. The system was calibrated with ion chamber dosimeter and Gafchromic™ EBT2 film with multichannel dosimetry. Detailed dosimetry determination can be found in our previously reported work (*16, 17*). The average dose rate at the mouse brain entrance plane has been measured to be 1.2 Gy/min. Peak dose at either 48 or 72 Gy was used for the low- or high-dose MRT protocol to irradiate the mouse brain. Each microbeam was 280 μm wide and 160 mm long, spaced at 900 μm center-to-center distance. Three microbeams of radiation were delivered unidirectionally across the mouse brain in the low-dose MRT group, while two microbeams were delivered in the high-dose MRT group, so the total integrated doses were the same in the two MRT groups. The orientation of the beam is shown in Fig. 1C. Microbeam profiles were validated by Gafchromic EBT2 films placed at the entrance and exit plane of the mouse head.

Image-guided MRT was performed according to previously reported protocol (*16*). Briefly, mice first underwent MRI for tumor localization, and were then transported to the radiation laboratory the next day for MRT. For radiation treatment, the animal was anesthetized with isoflurane (1.5%) mixed with 100% oxygen gas and placed in prone position on the mouse cradle for X-ray radiography imaging. MR images of the mouse head were then registered to the X-ray images using rigid body registration. The relative position of the tumor to the landmarks on the imaging bed was then determined from the registered image, and subsequently used to maneuver the imaging bed to the treatment position with a high-precision translation stage (Velmex Inc., Bloomfield, NY), so that the microbeam radiation could be accurately delivered to the tumor target.

A total of 57 tumor-bearing mice and six normal mice were treated with MRT for survival and immunostaining studies. In the survival study, 42 animals were distributed into three groups based on tumor size so that the average tumor size of each group was not statistically different from the other groups before treatment. The three groups included a sham-irradiated group (isoflurane only, no irradiation, n = 19), a low-dose MRT group treated with peak radiation dose of 48 Gy (n = 19) and a high-dose MRT group treated with peak radiation dose of 72 Gy (n = 4). Another batch of tumor-bearing mice (n = 15) and normal mice (n = 6) were used for immunostaining study after MRT (see the Immunostaining section).

Conventional Broad-Beam Radiation Treatment

A separate group of U87MG tumor-bearing mice (n = 17) underwent conventional broad-beam radiation treatment. Mice were anesthetized with the same isoflurane inhalation method and placed on the radiation treating bed. Radiation of 10 Gy was delivered to the mouse brain using a clinical linear accelerator (Siemens Primus, 6 MV photon beam). The radiation field is 1 × 1 cm centered on the mouse brain. The treatment dose was computed using in-house clinical treatment planning software PLUNC.

After irradiation, one group of mice (n = 9) was used to study survival by recording animal life span after treatment. Another group of mice (n = 8) was used for histological analysis by collecting brain tissue at 24 h (n = 4) and 48 h (n = 4) after irradiation.

Immunostaining and Quantification

Tumor-bearing mice were euthanized at 1, 4, 24, 48 h and day 7 after low-dose MRT or at 24 and 48 h after BRT. Brains were collected and fixed in formalin for 48 h. The fixed brains were then dehydrated, embedded in paraffin and cut into 5 μm brain sections in sagittal plane perpendicular to the microbeam direction near tumor location. The cutting location was determined from MR images. Three consecutive brain sections were used for staining with antibodies to phosphorylated histone γ-H2AX, cleaved caspase-3 and Ki-67 protein to assess DNA DSBs, apoptosis and cell proliferation, which have been well documented in the literature (*18, 19*). All immunostaining procedures were conducted in the Tissue Pathology Core Facility with standardized staining protocol for all the tissue slides and positive/negative slides. For staining, tissue sections were deparaffinized followed by antigen retrieval with citrate buffer, and incubated with primary antibodies to one of the following proteins: γ-H2AX (rabbit anti-mouse γ-H2AX antibody; Cell Signaling Technology®, Danvers, MA), 1:1,000 dilution, 8 h incubation; cleaved caspase-3 (Biocare Medical Inc., Concord, CA), 1:400 dilution, 4 h incubation); and Ki-67 (BD Pharmingen™, San Diego, CA), 1:500 dilution, 4 h incubation. The sections were then incubated with an appropriate secondary antibody followed with tyramide Cy5 amplification (PerkinElmer® Inc., Boston, MA). To stain nuclei and preserve the fluorescent signals, ProLong® Gold antifade reagent containing 4,6-diamidino-2-phenylindole (DAPI) was used (Molecular Probes®, Eugene, OR) on stained sections. The section was then scanned in the DAPI and Cy5 channels using a high-resolution (20× objectives) fluorescence slide scanner system (ScanScope FL scanner, Aperio®, Vista, CA). Immunostaining of γ-H2AX, caspase-3 and F4/80 (microglia and macrophage marker) was conducted on normal mouse brain tissues at 24 h and at day 30 after irradiation to assess both acute and chronic damage on normal tissue from microbeam radiation.

The γ-H2AX quantification method was based on a previously published study (*20*) where the positively stained γ-H2AX fluorescence signal in nuclei was confirmed to be correlated with the expressed γ-H2AX protein level measured by Western blot. To quantify the γ-H2AX signal, cell nucleus region was first extracted from the DAPI nuclei counterstaining channel and masked to the γ-H2AX Cy5 fluorescence channel. Since γ-H2AX foci were present solely in cell nuclei, only signals inside the cell nuclei were measured. This method prevented the possibility of bias caused by different cell density in tumor and normal brain tissue. Five regions were defined based on the γ-H2AX staining images: radiation beam passing regions on the tumor tissue (tumor peak region) and on the contralateral normal brain tissue (normal peak region), beam valley regions on the tumor tissue (tumor valley region) and normal brain tissue (normal valley region) and regions away from the MRT field as normal tissue background (normal tissue region). Average fluorescence signal on the masked nuclei area was measured as mean γ-H2AX signal for the five regions.

Apoptosis was detected using cleaved caspase-3 staining. The caspase-3 images were first aligned with the γ-H2AX images from the neighboring section using ImageJ software (version 1.47), and the five tissue regions defined in the γ-H2AX images were mapped to the caspase-3 images. Numbers of positively stained cells in peak and valley regions were counted in tumor and normal tissue. The number of positively caspase-3 stained cells per mm^2 was calculated as a quantitative measure of the apoptosis level after irradiation.

Immunofluorescence staining on Ki-67 protein was conducted on irradiated brain sections to measure cell proliferation. One tumor section from a sham-irradiated mouse was always included as a positive control. Area fraction of positive Ki-67 staining on the nuclei area was measured in the tumor peak and tumor valley regions. The ratio between irradiated tumor tissue and nonirradiated positive control was reported as the proliferation ratio. In the contralateral normal brain tissue, the number of

positively stained cells on the irradiated region in the middle of striatum of MRT mice and the same sized region of BRT mice was measured as the parameter to quantify normal tissue proliferation.

Statistical Analysis

Data from the survival studies were analyzed using the Kaplan-Meier method (GraphPad Prism software; GraphPad Software Inc., LaJolla, CA). The median survival time and the percentage of extended life span were reported. The extended life span is defined as the ratio of the extension of median survival time in the treated group to the median survival time in the control group. Survival curves were compared using the logrank test between each group. Data on expression level of γ-H2AX, caspase-3 and Ki-67 were presented as mean ± SEM. Differences between expression level on tumor and normal tissue at different time points after MRT were compared using *t* test. $P < 0.05$ was considered significant.

RESULTS

MRT on Mouse Brain and Radiation Dose Verification

The delivered microbeam radiation dose was verified using Gafchromic films placed at the entrance and exit planes of the mouse head. The beam width (full width at half maximum, FWHM) was 280 μm at the entrance plane on the top of the mouse brain and 380 μm at the exit plane at the bottom of the head. The peak-to-valley-dose-ratio (PVDR) was measured to be 16 at the entrance plane and decreased to 14 at the exit plane (see Fig. 2A and B).

Using γ-H2AX staining on irradiated brain tissue, we were able to clearly show the radiation beam tracks in normal brain tissue (Fig. 2C) and in tumor-bearing mouse brain (Fig. 2D). The center-to-center distance between two adjacent tracks in the γ-H2AX image was measured to be 782.2 μm on average, which was very close to the prescribed beam pitch of 900 μm when taking into consideration a ~20% tissue shrinkage during histology processing (*21*). The FWHM of the track was 343.4 μm in the γ-H2AX staining images, which was wider than the radiation beam width at the exit plane, considering the tissue shrinkage. This was possibly due to the nonlinear response between radiation dose and γ-H2AX expression at doses above 10 Gy (*22*), causing widened FWHM measurement on γ-H2AX expression tracks.

MRT on Overall Survival and Tumor Control

Median survival time (MST) for the sham-irradiated group was 35 days after tumor inoculation [95% CI = (34.4, 35.6)]. The MST for animals treated with low-dose MRT, high-dose MRT and BRT was 46 (43.2, 48.8) days, 52 (40.8, 63.2) days and 52 (50.9, 53.1) days (values shown in parentheses are 95% confidence interval) respectively, as shown in Fig. 3. Both low-dose and high-dose MRT significantly extended mouse life span ($P < 0.001$, logrank test) by 31.4 and 48.5%, respectively. The extended life span for the BRT group was 48.5%. There was no significant difference among the BRT group and the two MRT groups in terms of median survival time ($P > 0.05$, logrank test).

Tumor-bearing mice underwent MRI scans and tumor volumes were measured over time before and after radiation treatment. Figure 4A shows typical T2 weighted MR images from each group at different time points. Absolute tumor volume measurement for each group is shown in Fig. 4B. The volume change ratio, i.e., the tumor volume increase from the initial volume before MRT divided by the initial volume $[(V_t - V_0)/V_0]$, was calculated for individual animals and plotted in Fig. 4C. At one week after MRT, the sham-irradiated group had 10.0 ± 2.1 fold of increase in tumor volume, while the low-dose and high-dose MRT groups had only 4.1 ± 1.1 fold and 1.5 ± 0.8 fold of volume increase, respectively, demonstrating significant inhibition of tumor growth after MRT ($P < 0.01$ for both MRT groups and the sham-irradiated group). At day 14 after MRT, tumor volume was 51.7 ± 16.0, 37.0 ± 9.4 and 14.3 ± 4.1 fold of increase in the sham-irradiated, low-dose and high-dose MRT groups, respectively. Tumor growth was continuously suppressed (>10 times) by the high-dose MRT at a significant level ($P = 0.04$), while only a trend of inhibition was observed with low-dose MRT ($P = 0.21$).

MRT on DNA Damage and its Dynamics

Expression of γ-H2AX was measured at 1, 4, 24, 48 h and day 7 after MRT. Figure 5 shows γ-H2AX staining on both tumor and normal tissue in the contralateral hemisphere. Strong expression was observed as early as 1 h postirradiation on both tumor and normal tissue on the radiation beam passing regions, indicating radiation-induced DNA DSBs. The expression reduced over time from 1 h to day 7 after irradiation on both tumor and normal tissue, suggesting the ongoing repair process in response to DNA damage. By day 7 after irradiation, the γ-H2AX signal in the normal valley region dropped to background level, but the γ-H2AX signal in the tumor tissue did not. Average γ-H2AX signal in nuclei was quantified in the five regions, defined in the Materials and Methods section. In the radiation beam passing region, there was a trend of higher γ-H2AX level in tumor (tumor peak) compared to that in the normal brain tissue (normal peak) at all time points, however, it was not statistically significant, possibly due to high variation. In the radiation valley region, the γ-H2AX signal was initially similar between the tumor valley and normal valley regions, but showed significantly higher in tumor valley region starting at 24 h postirradiation. The signal in the tumor valley was 1.38-, 1.61- and 1.92-fold higher than that in the normal valley region at 24 and 48 h and day 7 after irradiation ($P = 0.045$, 0.038 and $P < 0.001$, respectively). More interestingly, the γ-H2AX signal differences between peak and valley regions in tumor reduced dramatically at 48 h and almost diminished at day 7 after irradiation. The signal ratio between peak and valley regions in tumor changed from 5.2 at 1 h after MRT to 2.3 at 48 h and 1.1 at day 7 after MRT. Figure 5A shows that the γ-H2AX foci were more dispersed from the beam tracks to the overall tumor region at 48 h and day 7 after irradiation.

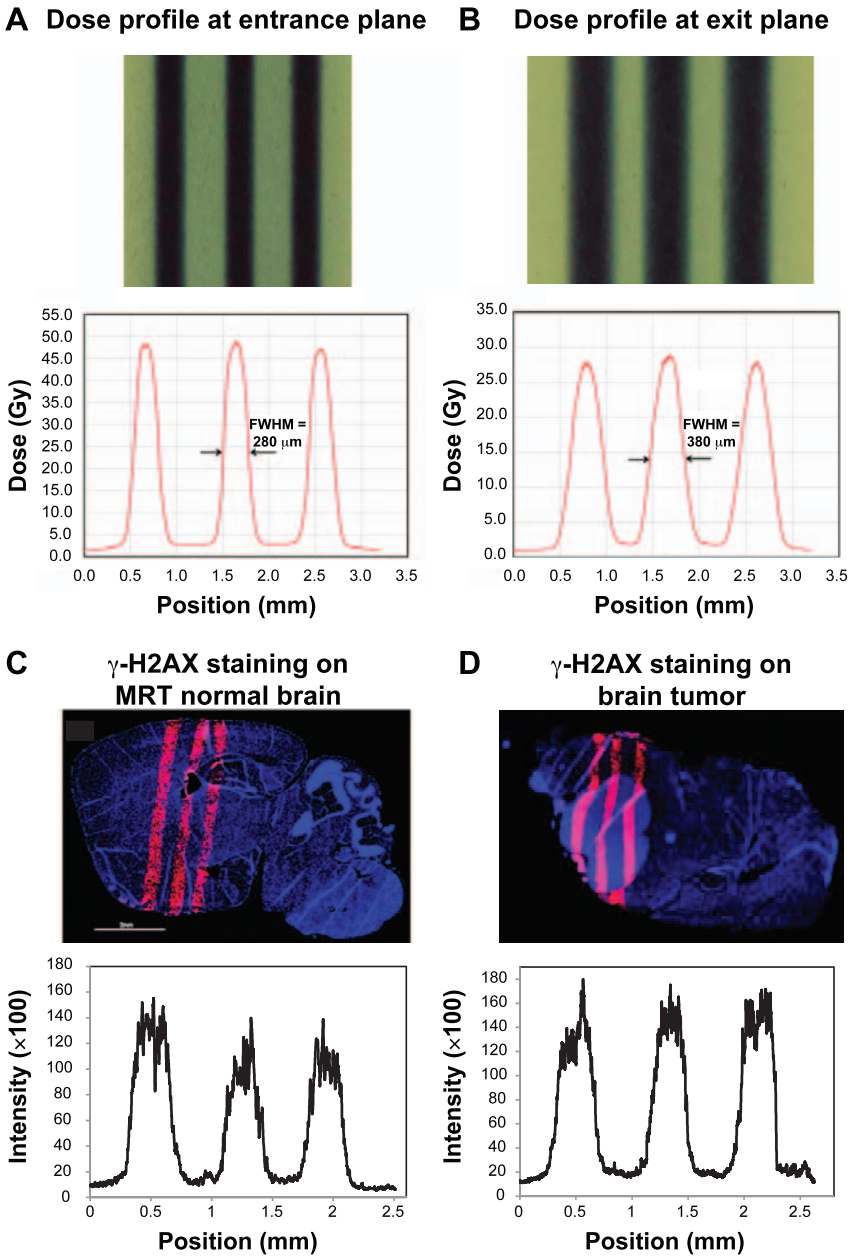

FIG. 2. Microbeam profiles using Gafchromic films and γ-H2AX staining on irradiated brain. The beam width (FWHM) was 280 μm at the entrance plane on the top of the mouse brain (panel A) and 380 μm at the exit plane at the bottom of the head (panel B). Normal brain tissue section (panel C) and tumor-bearing mouse brain (panel D) were stained with anti-γ-H2AX antibody at 1 h after microbeam irradiation. Red fluorescence signal indicates the positive expression of γ-H2AX signal. Staining of γ-H2AX demonstrated the microbeam radiation track. The average FWHM of the γ-H2AX staining was 343 μm.

In contrast, there were still clear separations between peak and valley regions at 48 h and day 7 after MRT in normal tissue, although the signal was quite weak at the 7-day time point. The spreading of γ-H2AX signal in the tumor might be caused by tumor cell migration and possible bystander effect.

MRT on Apoptosis and Cell Proliferation

Figure 6 shows the results of caspase-3 staining on tumor and normal brain tissue. In the tumor tissue, positive cleaved caspase-3 signal was initially low, but increased over time in both the tumor peak and tumor valley regions (Fig. 6A–C). Interestingly, the difference in apoptosis level between the peak and valley regions in the tumor decreased significantly at 48 h and at day 7 after irradiation. The ratio of apoptotic cells in the peak to that in the valley region was 2.3 at 4 h, dropping to 1.1 at day 7 after MRT (Fig. 6C). The number of apoptotic cells was (59 ± 12)/mm^2 in the peak region and (55 ± 14)/mm^2 in the valley region at day 7 in tumor tissue.

The number of apoptotic cells in contralateral normal brain tissue within the microbeam radiation field was

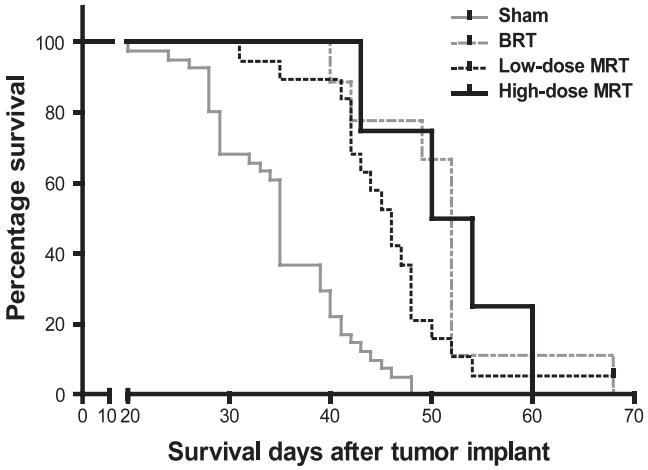

FIG. 3. Survival curves of four groups of U87MG-bearing mice, each with a different treatment. The groups received sham irradiation, low-dose MRT (48 Gy of peak dose, 280 μm beam width and 900 μm beam separation), high-dose MRT (72 Gy of peak dose, with the same beam width and separation) or BRT (10 Gy of conventional broad-beam radiation).

quantified after the low-dose MRT (Fig. 6D). Compared to the tumor tissue, there was a much lower level of apoptosis in the normal brain tissue after MRT. Apoptotic cells were mainly in the microbeam peak region with little to no apoptotic cells in the valley region (see Supplementary Fig. S1; http://dx.doi.org/10.1667/RR13919.1.S1). The number of apoptotic cells peaked at 24 h after MRT (0.66 ± 0.12/mm^2) and reduced thereafter in the normal brain tissue. Apoptosis level was also assessed in normal brain tissue at 24 and 48 h after BRT, and was significantly higher (0.65 ± 0.11/mm^2) compared with that in the MRT group (0.35 ± 0.09 /mm^2) at 48 h after irradiation.

Proliferation measurement with Ki-67 staining showed that tumor proliferation was significantly reduced in the radiation beam passing region at 1 h after irradiation (average of 15% drop from the nonirradiated control level), and continued to drop at 4, 24 and 48 h after irradiation (average of 27, 50 and 70% drop, respectively), as shown in Fig. 7. Tumor cells in the valley dose region had a lower reduction on proliferation compared to the radiation beam passing region (3, 9, 28 and 43% drop at 1, 4, 24, and 48 h after MRT, respectively). However, at day 7 after MRT, tumor proliferation returned to the level similar to that at 4 h postirradiation. The radiation beam passing region and radiation valley region at day 7 had averages of 77 and 83% proliferation levels compared to the nonirradiated tumor tissue, suggesting tumor regrowth after MRT.

In the contralateral normal tissue, there was an increase of cell proliferation after MRT, which peaked at 48 h (Fig. 8). The proliferation cells were found mainly in the valley region in the MRT field (see Supplementary Fig. S2; http://dx.doi.org/10.1667/RR13919.1.S1). Compared to the normal brain tissue after BRT, there was a dramatically higher level of cell proliferation in the MRT-treated normal tissue (7.43 ± 2.09/mm^2 and 10.64 ± 3.41/mm^2 for 24 and 48 h, respectively, for the MRT vs. 0.51 ± 0.11/mm^2 and 0.50 ± 0.11/mm^2 for 24 and 48 h, respectively, for the BRT), which was more than 20 times higher at 48 h after irradiation. This higher proliferation level in the normal brain tissue after MRT suggests a rapid tissue regeneration process after MRT.

Normal mice without tumor were irradiated with the low-dose MRT protocol in the forebrain region, and expression of γ-H2AX, caspase-3 and F4/80 on normal brain tissue was examined at 24 h and day 30 after MRT. Thirty days after MRT, there were no obvious γ-H2AX signal tracks,

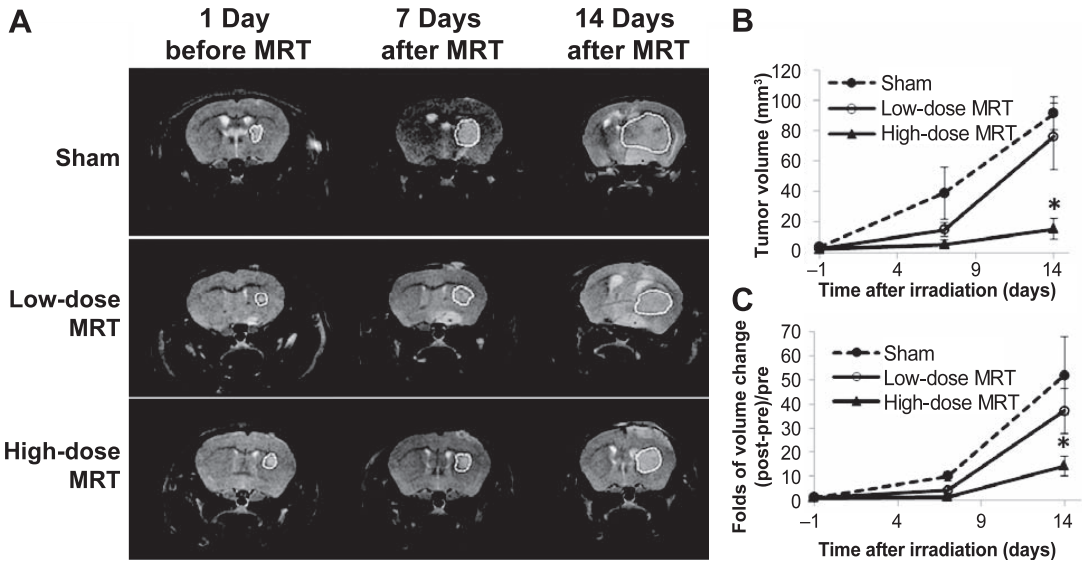

FIG. 4. Tumor volume measurement using MRI before and after microbeam irradiation. Panel A: T2 weighted MR images at different time points for the three groups. The white dashed line shows the tumor region contours. Panels B and C: Absolute tumor volume measurement and volume changes, respectively. Tumor volume was significantly suppressed at day 7 after irradiation in two treatment groups. At day 14 after irradiation, tumor volume in the high-dose MRT group was significantly lower than that in the sham-irradiated group (*$P = 0.04$). Low-dose MRT only showed a trend of tumor suppression at day 14 after irradiation ($P = 0.21$).

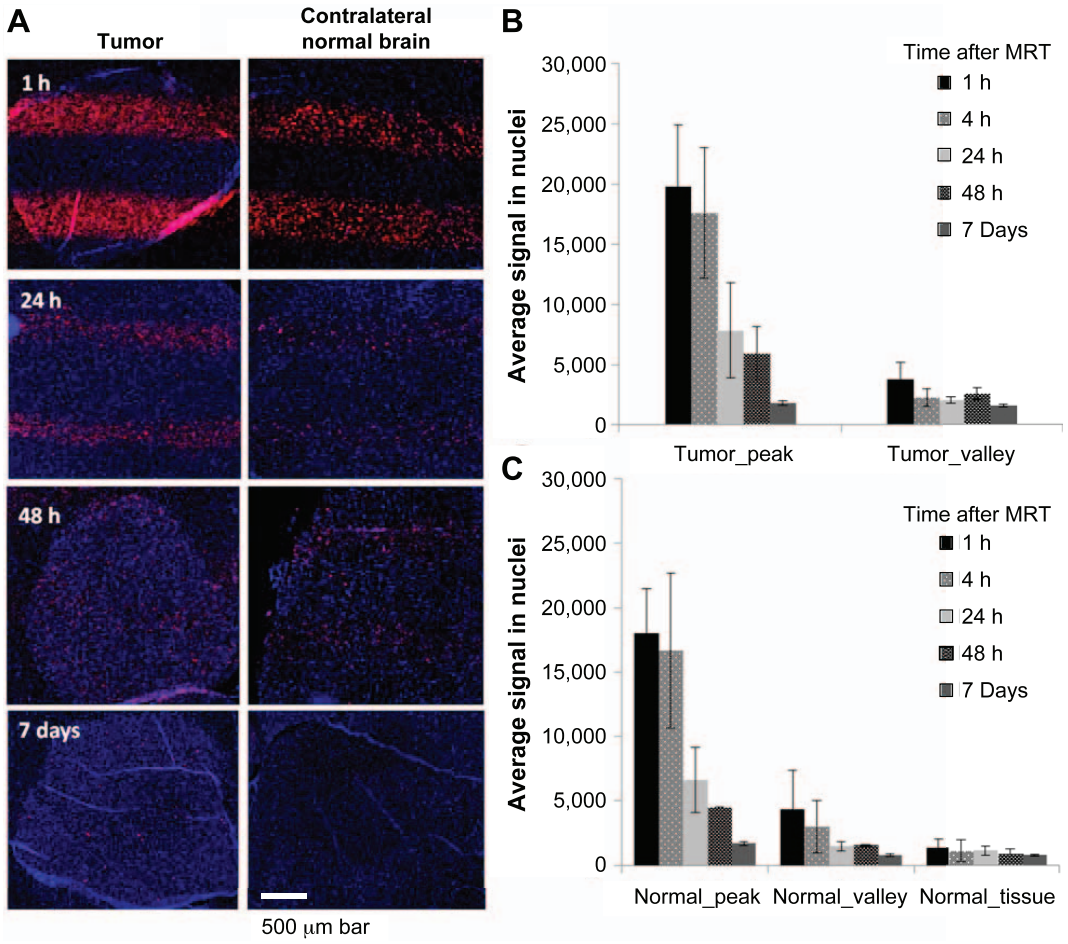

FIG. 5. Gamma-H2AX staining on irradiated tumor and normal brain tissue. Panel A: Changes of γ-H2AX signal at different times after MRT on tumor and normal brain tissue. Microbeam radiation paths were clearly shown at 1 and 24 h, however, the peak and valley tracks became mixed at 48 h and day 7 on tumor tissue, but not on normal brain tissue. Panels B and C: Quantified γ-H2AX levels. The expression of γ-H2AX reduced over time, indicating a repair process after irradiation. The expression level was similar in the peak region between tumor and normal tissue, however, there was significantly higher expression of γ-H2AX in the tumor valley region compared to that in the normal valley region at 24 h, 48 h and day 7 after MRT.

however, low γ-H2AX staining signal was found sporadically in the irradiated region. The apoptosis level at 24 h after MRT on normal mouse brain was 0.41 ± 0.07/mm^2, which was much lower than the level at the contralateral normal brain tissue in the tumor mice (0.66 ± 0.12/mm^2) ($P = 0.08$). Thirty days after MRT, the apoptosis level in the irradiated region dropped to its lowest (0.18 ± 0.04/mm^2) compared to all time points examined.

Neither microglial activation nor macrophage infiltration was found on normal brain at 24 h or day 30 after irradiation, as shown in F4/80 staining images (Fig. 9). There was some nonspecific F4/80 staining in the neuron cells, but no positive staining in microglial or macrophages compared to a positive control.

DISCUSSIONS AND CONCLUSIONS

This work demonstrates the feasibility of conducting MRT studies on a glioblastoma multiforme tumor mouse model using the compact CNT-based image-guided microbeam irradiator in a regular laboratory setup. Although this first-generation device was not ready to generate the ultra-high dose of hundreds Gy used in synchrotron-based MRT studies, it has allowed us to produce a typical microbeam radiation profile and evaluate the MRT effects on both tumor and normal tissue. Our initial assessment showed that even at the relatively low-dose level the life span in the two MRT protocol-treated tumor mouse groups was significantly extended compared to the nontreated, sham-irradiated group. Although more than half of the tumor volume was in the valley dose regions, which received lower dose radiation (less than 5 Gy, calculated with the average PVDR of 15), the MRT group showed survival similar to that of the 10 Gy BRT group. Tumor volume growth was greatly suppressed in the high-dose MRT group in the two-week monitoring period after irradiation, although it did not result in a significant extension of survival compared to the low-dose MRT and BRT group. Mice treated with low-dose MRT

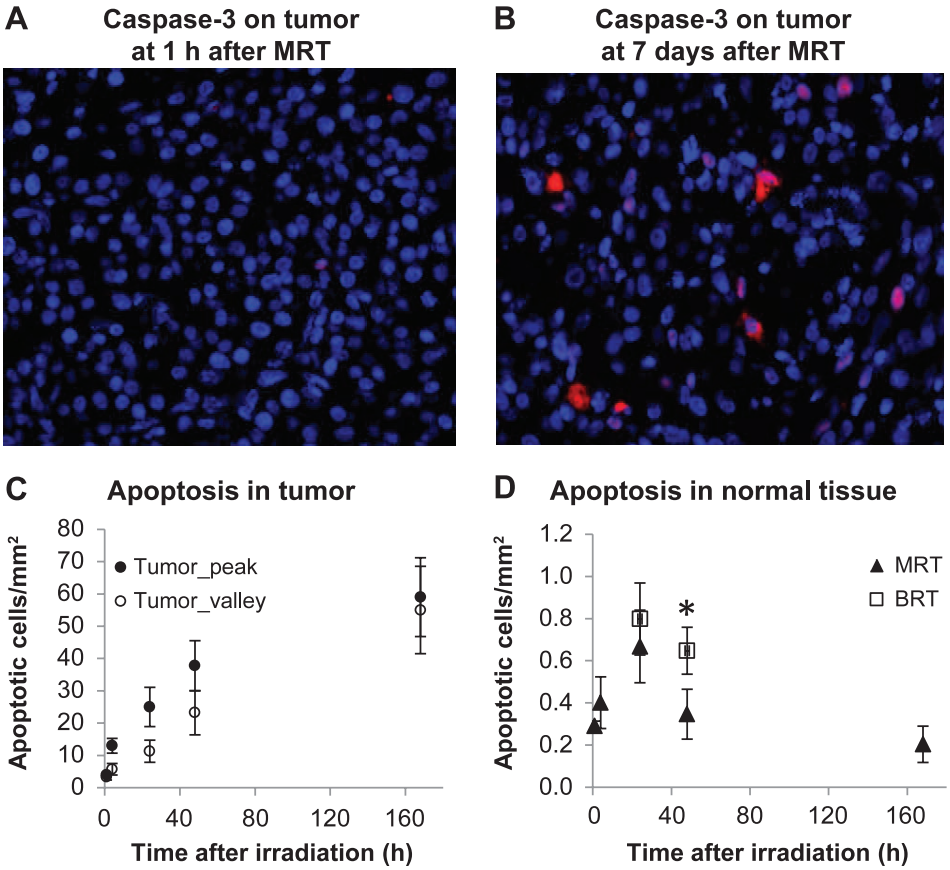

FIG. 6. Immunofluorescence staining of cleaved caspase-3 as cell apoptosis assay. Cleaved caspase-3 signal is shown in red fluorescence. Red: positively stained cleaved caspase-3 signal; blue: DAPI counterstaining of the nuclei. Panel A: Low level of apoptosis at 1 h after MRT in tumor tissue. Panel B: Apoptotic cells at day 7 after MRT in tumor tissue. Panel C: Number of apoptotic cells from 1 h to day 7 after MRT in tumor tissue. There were significant differences between the peak and valley regions at 4 and 24 h, but not at 48 h and day 7 after MRT. Panel D: Number of apoptotic cells in the contralateral normal brain tissue after MRT and at 24 and 48 h after BRT. There was a significantly higher level of apoptosis at 48 h after BRT (*$P < 0.05$, compared to MRT).

had initial tumor suppression, with tumor regrowth at a later phase, which was consistent with the Ki-67 staining of tumor proliferation. Immunostaining of γ-H2AX and cleaved caspase-3 showed higher DNA damage and more apoptosis in tumor tissue compared to normal brain tissue. MRT on normal brain tissue caused low apoptosis and little macrophage infiltration at 30 days after exposure, indicating that normal brain tissue tolerates well with prescribed MRT.

As a first-generation prototype the performance of the current device is far from reaching the full potential of the distributed X-ray source array as a compact MRT irradiator. However, we have demonstrated that it is capable of generating microbeam radiation with MRT dosimetric characteristics, including beam width and PVDR, which are proven effective as MRT regimen. Although other studies have shown high therapeutic efficacy with normal-tissue-sparing effect using synchrotron MRT (*6, 8*), it is pivotal to evaluate the MRT effects on animal models with this compact MRT system, given the differences in MRT parameters among the systems. The microbeam width used in the current MRT study was 280 μm, which is wider than the ones typically used in the early synchrotron MRT studies (25–90 μm). The width of the microbeam generated by the compact CNT-MRT is determined by the beam-forming collimator, which is adjustable in width, and the width of the X-ray focal line, which is 130 μm in the current system. Dilmanian *et al*. proposed a so-called ''mini-beam radiation concept'', where radiation beams as thick as 0.68 mm were used for treatment, and demonstrated good normal tissue sparing in the rat CNS with dose up to 170 Gy (*23, 24*). Several other studies have also reported the tissue sparing effect and tumoricidal results from radiation beams with about 0.6 mm thickness (*5, 25*). These studies show that it is not necessary to limit the radiation beam width below 100 μm to retain normal tissue sparing and tumor control. Our results and those of others with wider beam width make more promising the potential clinical application of MRT, and also make it more feasible to achieve high-dose rate in our compact MRT technology.

One limitation of our current MRT system is its relatively low dose rate. The current system delivers at an average microbeam dose rate of 1.2 Gy/min, which limits the total

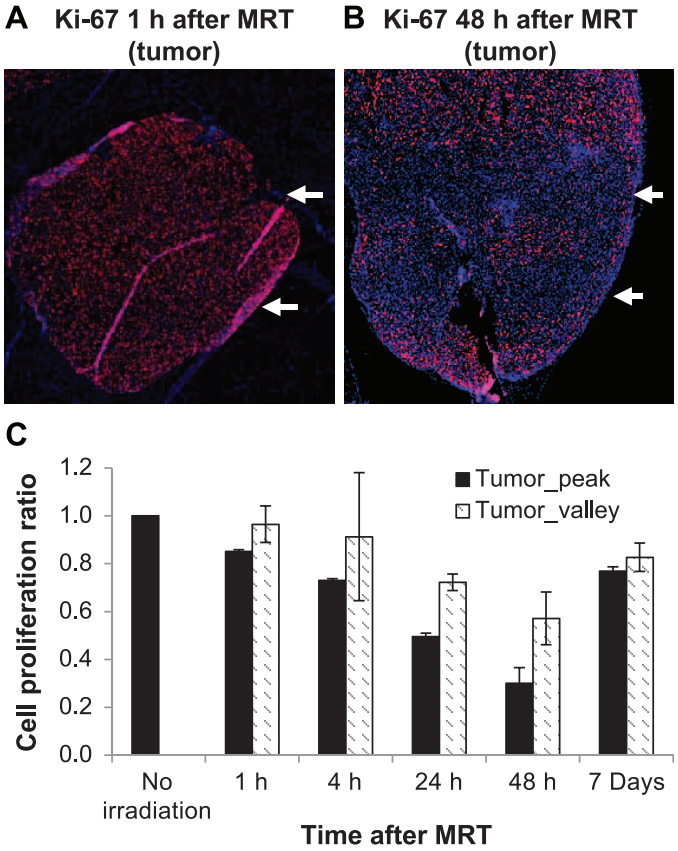

FIG. 7. Immofluorescence staining of Ki-67 as cell proliferation assay on tumor after MRT. Examples of Ki-67 staining on tumor tissue at 1 h (panel A) and 48 h (panel B) after MRT are shown. Red: positively stained Ki-67 protein associated with cell proliferation; blue: DAPI counterstaining of the nuclei. White arrows indicate the radiation beam direction on the tumor tissue. Ratios of proliferation staining to nonirradiated control are plotted over time for both the tumor peak and tumor valley region (panel C). The proliferation continuously decreased in both radiation peak and valley regions from 1 to 48 h, however, it bounced back at day 7 after MRT.

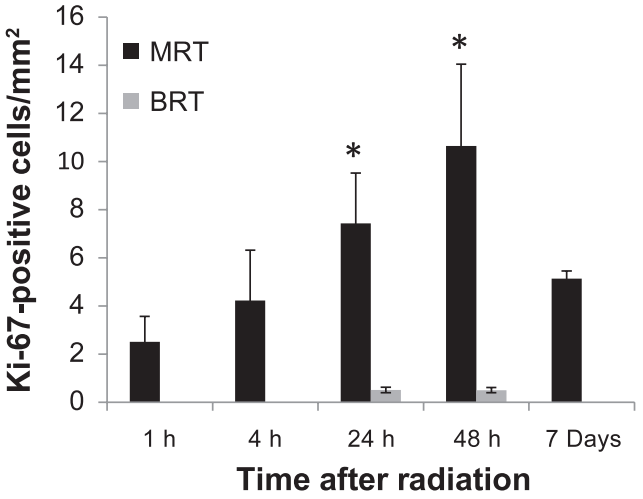

FIG. 8. Number of Ki-67-stained proliferation cells on the contralateral normal brain tissue after MRT and BRT. A significantly higher number of proliferation cells were found in the MRT mice, but not in the BRT mice at 24 and 48 h after irradiation (*$P < 0.05$, compared to BRT).

dose that can be delivered to an anesthetized animal in the experiment. The peak doses used in the two MRT protocols were 48 and 72 Gy, much lower than peak doses used in a typical MRT study in the synchrotron facility. Although we have not conducted many animal studies with high-dose MRT due to the limited low dose rate, we have demonstrated that both MRT protocols extended the life span of tumor-bearing mice (48.5% and 31.4% increase of life span for high- and low-dose MRT, respectively). A similar outcome has been reported in synchrotron-based MRT research. Prezado *et al.* recently reported an increased life span of about 42% on 9L glioma rats treated with unidirectional MRT (as used in this study) with 100 Gy peak dose, 640 μm beam width and 1.12 mm center-to-center distance (*5*). In their study, the life span was further increased to 100% when an interlaced microbeam pattern was applied. Nevertheless, we recognize the need to place dose rate as a top priority in compact MRT technology development and anticipate that the second generation CNT MRT system (under construction) will have a 20× increase in dose rate.

Our study showed that there was low level of normal tissue damage in normal mouse brain after MRT with the presented radiation dosage. There was significantly lower number of apoptotic cells at 48 h after MRT compared to that after 10 Gy BRT. A low level of apoptosis and no F4/80$^+$ macrophages were observed at 24 h or day 30 after MRT in normal mouse brain, indicating good tolerance of brain tissue to the prescribed MRT. Our current assessment on the normal tissue damage is limited to DNA damage and apoptosis in this article. More physiological and functional assays including blood-brain-barrier and inflammation measurement have been planned out and will be included in a future study.

Radiation-induced normal tissue damage has been well documented in conventional radiation treatment. It has been reported that radiation exposure could cause a significant amount of apoptosis in rodent brain, especially at the dentate subgranular zone (SGZ) in a dose-dependent manner after whole-brain irradiation (*26, 27*). Neuro-inflammation has been reported after whole-brain single-dose irradiation and manifested as activated astrocytes, activated microglial cells and infiltrated macrophages, as early as 4 h *in vivo* (*28, 29*) and as late as 1 month and 6 months after whole-brain irradiation (*30–32*). Morganti *et al.* reported a significant increase in F4/80$^+$ activated macrophages in irradiated brains compared to sham-irradiated brains at day 7, 14 and 28 after 10 Gy cranial irradiation (*32*). Moravan *et al.* reported acute neuro-inflammation at day 3 after 35 Gy irradiation, and delayed microglia activation and T-cell infiltration at 1 month after $\geq$15 Gy irradiation (*30*). On the other hand, many studies have demonstrated normal tissue-sparing effects from the MRT. Laissue *et al.* first reported unexpected minor damage to normal brain tissue after high-dose MRT (312 and 625 Gy peak dose, 100 μm width) (*9*). Priyadarshika *et al.* reported significantly less skin damage, including leukocyte

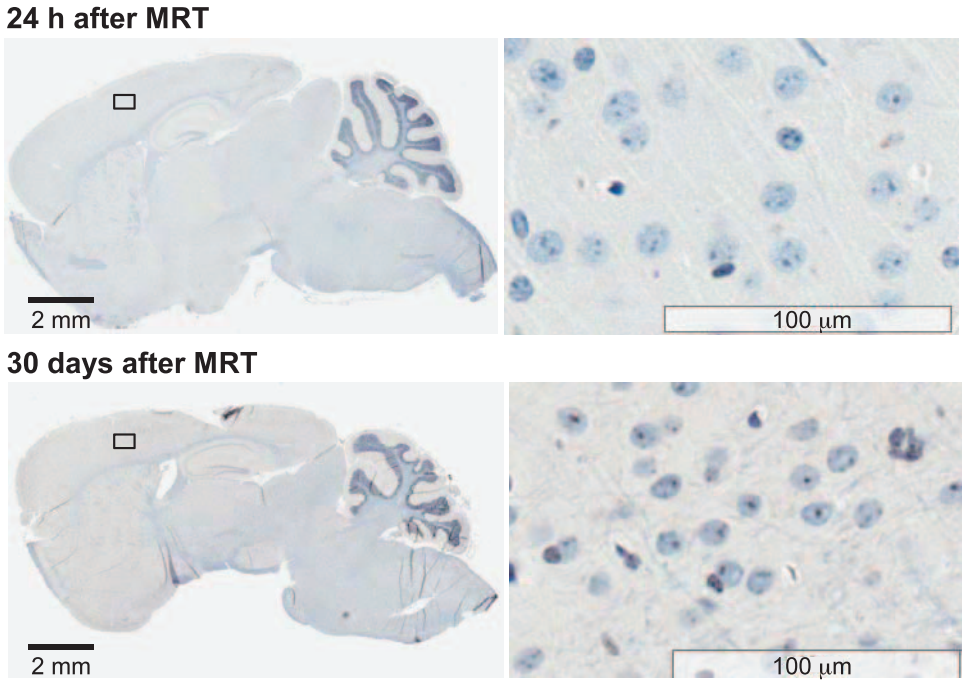

FIG. 9. Immunohistochemistry staining of F4/80 on normal brain tissue at 24 h and day 30 after MRT. There were no positively stained macrophages or microglial cells found at either 24 h or day 30 after MRT. No other morphological brain tissue damage was detected.

infiltration, from high-dose MRT (800 Gy) than from high-dose (44 Gy) BRT (*33*). Dilmanian *et al*. reported a study with MRT on duck embryonic brain and demonstrated that brain tolerance to microbeam irradiation was about three times higher than to broad-beam irradiation. There were few radiation-induced lesions observed with a microbeam dose of 40–160 Gy in the peak (*11*). MRT (270 μm beam width, peak dose of 750 Gy) in a rat spinal cord study resulted in a loss of oligodendrocytes and myelin in two weeks postirradiation, but repopulation and re-myelination was nearly complete in 3 months after MRT. Although ''dose-volume effect'' [i.e., tissue-tolerant dose increases when radiation volume gets smaller (*10, 34*)] has been a general explanation, detailed molecular mechanisms and signal pathways to explain how normal tissue recovers efficiently from MRT have not been well established. Serduc *et al*. reported low damage and quick recovery on the brain vasculature and blood–brain barrier after low-dose (350 Gy) MRT, and transient blood–brain barrier breakdown after high-dose (1,000 Gy) MRT using either intravital microscopy (*35*) or MR imaging methods (*36*). While this rapid recovery of normal vascular system has been considered to be the major contributor to the normal tissue-sparing effects after MRT, further mechanistic studies to elucidate the vascular repair process are still needed.

It is hypothesized that normal microvessels damaged in the beam path can regenerate quickly while tumor vasculature cannot due to structural and molecular differences of the tumor vessels (*37, 38*). Dilmanian *et al*. also proposed beneficial bystander effects through the release of the growth factors after MRT, promoting proliferation, migration and differentiation of the progenitor glial cells to produce new functional glial cells (*39*). However, the exact pathway, dynamics and essential molecular elements of bystander effects still require extensive investigation. Our results showed more than 20× higher cell proliferation found in the microbeam-treated normal brain compared to broad-beam-treated normal tissue. Crosbie *et al*. reported that normal skin tissue showed increased proliferation starting from 48 h after MRT as one of the tissue-repairing processes (*40*). In our study, we observed an increase in Ki-67-positive cells beginning at 24 h and continuing 48 h after MRT of the brain, indicating rapid tissue regeneration and repair from MRT. The mechanisms of normal tissue repair and regeneration warrant further investigation.

One interesting finding in this present study is the spreading of the γ-H2AX expression from the radiation peak region to the valley region at 48 h and day 7 after irradiation. We also observed that apoptotic cells were distributed over the entire irradiated tumors at later time points and not confined within the radiation beam path. Although the ratio of apoptosis in general is relatively low compared to other cell lines after radiation treatment (*41*), the distribution of the apoptotic cells can be clearly observed. Two mechanisms that might be attributed to this phenomenon are cell migration or bystander effect. Crosbie *et al*. reported on the different responses between tumor cells and normal tissue, with results showing that the irradiated peak and valley zones were indistinguishable in tumors because of extensive cell migration between the

zones (*40*). Sprung *et al*. also reported that γ-H2AX foci at later time points did not directly correspond with the targeted regions, suggesting cell movement or bystander effects as a potential mechanism for MRT effectiveness. Kashino *et al*. showed that the induction of DNA DSBs and cell migration in glioma cells exposed to MRT *in vitro* were mediated by bystander effects (*42*). Our results are highly consistent with those studies in terms of indistinguishable damage in tumor tissue. However, extensive mechanistic studies are needed in the future.

We have compared the survival time and normal tissue damage between broad-beam and microbeam radiation exposure. Due to the much more complex dosimetry in MRT, biological equivalence of a MRT dose to a seamless BRT dose for a given tissue is still poorly understood. Priyadarshika *et al*. suggested that the integrated dose of MRT, which is the microbeam dose averaged over the entire radiation volume, might be more relevant than the peak or valley dose when compared to broad-beam radiation (*33*). Recently, Ibahim *et al*. conducted serial cell irradiation studies to evaluate the equivalence between synchrotron MRT and conventional BRT, and reported that BRT doses of 3.4 ± 0.1 Gy were radiobiologically equivalent to a peak microbeam dose of 112 Gy (25 μm wide spaced, 175 μm on center) using clonogenic assays on EMT6.5ch cells (*43*), which is much lower than the integrated MRT dose. On the other hand, the *in vitro* cell radiation study could not truly represent *in vivo* irradiation where possible bystander effects and vascular network factors might greatly influence the final efficacy. It is still debatable which dose level of broad-beam radiation can be used for a comparison with the MRT study. The dose level of 10 Gy was chosen for BRT in the study mainly because it has been widely used in small animal studies with single-fraction conventional radiation (*38, 43, 44*). Our study showed that 10 Gy of BRT led to a survival extension similar to MRT. However, our histology study indicated that BRT might cause more normal brain tissue damage than MRT. Apoptosis doubled at 48 h in normal brain tissue after BRT compared to MRT, although apoptosis levels in both BRT and MRT groups were very low ($0.65 \pm 0.11/mm^2$ vs. $0.35 \pm 0.09 /mm^2$, respectively). In addition, Ki-67 staining revealed the number of proliferating cells to be 20× higher in the normal tissue after MRT than after BRT, indicating much more rapid tissue repairing and recovery after MRT, and thus low damage to normal tissue functionality. Future studies to compare MRT to the clinical standard of care for glioblastoma, i.e., the combination of fractionation radiation and temozolomide (*45*), will be needed for a more clinically relevant comparison in terms of therapeutic efficacy.

The current study is the first to evaluate the radiobiological effects on mouse brain tumor using the newly developed prototype compact CNT-based image-guided MRT system. This study demonstrated that the MRT delivered by this compact system produces results in survival, tumor control and normal brain tissue sparing that are consistent with results from synchrotron-generated MRT studies. The findings from this study warrant continued development of compact MRT technology for mechanistic studies of this promising therapy.

SUPPLEMENTARY INFORMATION

Fig. S1. Apoptosis in normal brain tissue after microbeam radiation.

Fig. S2. Proliferation in normal brain tissue after microbeam radiation.

ACKNOWLEDGMENTS

The authors would like to thank the BRIC Small Animal Imaging Facility for providing MRI imaging services for the study, and the Tissue Pathology Laboratory for providing immunostaining and histological scanning. Both core facilities are supported in part by the National Cancer Institute (NCI), cancer center grant no. P30-CA016086-35-37. The current work is supported by the NCI-funded Carolina Center for Cancer Nanotechnology Excellence (no. U54-CA151652). The development of the compact MRT system was partially supported by a grant from the NCI ''Grand Opportunities'' Program (RC2-CA148487), and a pilot grant from the North Carolina Translational and Clinical Sciences Institute funded by NCRR (no. UL1RR025747). The authors would like to acknowledge Drs. Ryan Miller and Joel Tepper of UNC for helpful discussions and assistance and Rachel Ger for assistance in some of the experiments.

Received: September 22, 2014; accepted: July 9, 2015; published online: August 25, 2015

REFERENCES

1. Krex D, Klink B, Hartmann C, von Deimling A, Pietsch T, Simon M, et al. Long-term survival with glioblastoma multiforme. Brain 2007; 130 (Pt 10):2596–606.
2. Jovcevska I, Kocevar N, Komel R. Glioma and glioblastoma - how much do we (not) know? Mol Clin Oncol 2013; 1:935–41.
3. Stone HB, Coleman CN, Anscher MS, McBride WH. Effects of radiation on normal tissue: consequences and mechanisms. Lancet Oncol 2003; 4:529–36.
4. Prasanna PG, Ahmed MM, Stone HB, Vikram B, Mehta MP, Coleman CN. Radiation-induced brain damage, impact of Robbins' work and the need for predictive biomarkers. Int J Radiat Biol 2014; 90:742–52.
5. Prezado Y, Sarun S, Gil S, Deman P, Bouchet A, Le Duc G. Increase of lifespan for glioma-bearing rats by using minibeam radiation therapy. J Synchrotron Radiat 2012; 19 (Pt 1):60–5.
6. Schultke E, Juurlink BH, Ataelmannan K, Laissue J, Blattmann H, Brauer-Krisch E, et al. Memory and survival after microbeam radiation therapy. Eur J Radiol 2008; 68 (3 Suppl):S142–6.
7. Serduc R, Bouchet A, Brauer-Krisch E, Laissue JA, Spiga J, Sarun S, et al. Synchrotron microbeam radiation therapy for rat brain tumor palliation-influence of the microbeam width at constant valley dose. Phys Med Biol 2009; 54:6711–24.
8. Dilmanian FA, Button TM, Le Duc G, Zhong N, Pena LA, Smith JA, et al. Response of rat intracranial 9L gliosarcoma to microbeam radiation therapy. Neuro Oncol 2002; 4:26–38.
9. Laissue JA, Geiser G, Spanne PO, Dilmanian FA, Gebbers JO, Geiser M, et al. Neuropathology of ablation of rat gliosarcomas and contiguous brain tissues using a microplanar beam of synchrotron-wiggler-generated X rays. Int J Cancer 1998; 78:654–60.
10. Laissue JA, Blattmann H, Di Michiel M, Slatkin DN, Lyubimova N, Guzman R, et al. The weanling piglet cerebellum: a surrogate for tolerance to MRT (microbeam radiation therapy) in pediatric neuro-oncology. P Soc Photo-Opt Ins 2001; 4508:65–73.

11. Dilmanian FA, Morris GM, Le Duc G, Huang X, Ren B, Bacarian T, et al. Response of avian embryonic brain to spatially segmented x-ray microbeams. Cell Mol Biol 2001; 47:485–93.
12. Zhang J, Yang G, Cheng Y, Gao B, Qiu Q, Lee YZ, et al. Stationary scanning x-ray source based on carbon nanotube field emitters. Appl Phys Lett 2005; 86:184104.
13. Calderon-Colon X, Geng H, Gao B, An L, Cao G, Zhou O. A carbon nanotube field emission cathode with high current density and long-term stability. Nanotechnology 2009; 20:325707.
14. Hadsell M, Zhang J, Laganis P, Sprenger F, Shan J, Zhang L, et al. A first generation compact microbeam radiation therapy system based on carbon nanotube X-ray technology. Appl Phys Lett 2013; 103:183505.
15. Chtcheprov P, Burk L, Yuan H, Inscoe C, Ger R, Hadsell M, et al. Physiologically gated microbeam radiation using a field emission x-ray source array. Med Phys 2014; 41:081705.
16. Zhang L, Yuan H, Burk LM, Inscoe CR, Hadsell MJ, Chtcheprov P, et al. Image-guided microbeam irradiation to brain tumour bearing mice using a carbon nanotube x-ray source array. Phys Med Biol 2014; 59:1283–303.
17. Hadsell MJ. The development and characterization of a first generation carbon nanotube x-ray based microbeam radiation therapy system. ProQuest: University of North Carolina at Chapel Hill; 2013. (http://gradworks.umi.com/35/94/3594169.html)
18. Mariotti LG, Pirovano G, Savage KI, Ghita M, Ottolenghi A, Prise KM, et al. Use of the gamma-H2AX assay to investigate DNA repair dynamics following multiple radiation exposures. PLoS One 2013; 8:e79541.
19. Zarnescu O, Brehar FM, Chivu M, Ciurea AV. Immunohistochemical localization of caspase-3, caspase-9 and Bax in U87 glioblastoma xenografts. J Mol Histol 2008; 39:561–9.
20. Nikolaishvilli-Feinberg N, Cohen SM, Midkiff B, Zhou Y, Olorvida M, Ibrahim JG, et al. Development of DNA damage response signaling biomarkers using automated, quantitative image analysis. J Histochem Cytochem 2014; 62:185–96.
21. Winsor L. Tissue processing laboratory histopathology. In: Woods A, Ellis R, editors. Laboratory histopathology. New York: Churchill Livingstone; 1994.
22. Banath JP, Macphail SH, Olive PL. Radiation sensitivity, H2AX phosphorylation, and kinetics of repair of DNA strand breaks in irradiated cervical cancer cell lines. Cancer Res 2004; 64:7144–9.
23. Dilmanian FA, Zhong Z, Bacarian T, Benveniste H, Romanelli P, Wang R, et al. Interlaced x-ray microplanar beams: a radiosurgery approach with clinical potential. Proc Natl Acad Sci U S A 2006; 103:9709–14.
24. Dilmanian FA, Romanelli P, Zhong Z, Wang R, Wagshul ME, Kalef-Ezra J, et al. Microbeam radiation therapy: tissue dose penetration and BANG-gel dosimetry of thick-beams' array interlacing. Eur J Radiol 2008; 68(3 Suppl):S129–36.
25. Deman P, Vautrin M, Edouard M, Stupar V, Bobyk L, Farion R, et al. Monochromatic minibeams radiotherapy: from healthy tissue-sparing effect studies toward first experimental glioma bearing rats therapy. Int J Radiat Oncol Biol Phys 2012; 82:e693–700.
26. Andres-Mach M, Rola R, Fike JR. Radiation effects on neural precursor cells in the dentate gyrus. Cell Tissue Res 2008; 331:251–62.
27. Mizumatsu S, Monje ML, Morhardt DR, Rola R, Palmer TD, Fike JR. Extreme sensitivity of adult neurogenesis to low doses of X-irradiation. Cancer Res 2003; 63:4021–7.
28. Kyrkanides S, Olschowka JA, Williams JP, Hansen JT, O'Banion MK. TNF alpha and IL-1beta mediate intercellular adhesion molecule-1 induction via microglia-astrocyte interaction in CNS radiation injury. J Neuroimmunol 1999; 95:95–106.
29. Hwang SY, Jung JS, Kim TH, Lim SJ, Oh ES, Kim JY, et al. Ionizing radiation induces astrocyte gliosis through microglia activation. Neurobiol Dis 2006; 21:457–67.
30. Moravan MJ, Olschowka JA, Williams JP, O'Banion MK. Cranial irradiation leads to acute and persistent neuroinflammation with delayed increases in T-cell infiltration and CD11c expression in C57BL/6 mouse brain. Radiat Res 2011; 176:459–73.
31. Rola R, Raber J, Rizk A, Otsuka S, VandenBerg SR, Morhardt DR, et al. Radiation-induced impairment of hippocampal neurogenesis is associated with cognitive deficits in young mice. Exp Neurol 2004; 188:316–30.
32. Morganti JM, Jopson TD, Liu S, Gupta N, Rosi S. Cranial irradiation alters the brain's microenvironment and permits CCR2+ macrophage infiltration. PLoS One 2014; 9:e93650.
33. Priyadarshika RC, Crosbie JC, Kumar B, Rogers PA. Biodosimetric quantification of short-term synchrotron microbeam versus broad-beam radiation damage to mouse skin using a dermatopathological scoring system. Br J Radiol 2011; 84:833–42.
34. Withers HR, Taylor JM, Maciejewski B. Treatment volume and tissue tolerance. Int J Radiat Oncol Biol Phys 1988; 14:751–9.
35. Serduc R, Verant P, Vial JC, Farion R, Rocas L, Remy C, et al. In vivo two-photon microscopy study of short-term effects of microbeam irradiation on normal mouse brain microvasculature. Int J Radiat Oncol Biol Phys 2006; 64:1519–27.
36. Serduc R, van de Looij Y, Francony G, Verdonck O, van der Sanden B, Laissue J, et al. Characterization and quantification of cerebral edema induced by synchrotron x-ray microbeam radiation therapy. Phys Med Biol 2008; 53:1153–66.
37. Brauer-Krisch E, Serduc R, Siegbahn EA, Le Duc G, Prezado Y, Bravin A, et al. Effects of pulsed, spatially fractionated, microscopic synchrotron X-ray beams on normal and tumoral brain tissue. Mutat Res 2010; 704:160–6.
38. Sabatasso S, Laissue JA, Hlushchuk R, Graber W, Bravin A, Brauer-Krisch E, et al. Microbeam radiation-induced tissue damage depends on the stage of vascular maturation. Int J Radiat Oncol Biol Phys 2011; 80:1522–32.
39. Dilmanian FA, Qu Y, Feinendegen LE, Pena LA, Bacarian T, Henn FA, et al. Tissue-sparing effect of x-ray microplanar beams particularly in the CNS: is a bystander effect involved? Exp Hematol 2007; 35 (4 Suppl 1):69–77.
40. Crosbie JC, Anderson RL, Rothkamm K, Restall CM, Cann L, Ruwanpura S, et al. Tumor cell response to synchrotron microbeam radiation therapy differs markedly from cells in normal tissues. Int J Radiat Oncol Biol Phys 2010; 77:886–94.
41. Hara S, Nakashima S, Kiyono T, Sawada M, Yoshimura S, Iwama T, et al. p53-Independent ceramide formation in human glioma cells during gamma-radiation-induced apoptosis. Cell Death Differ 2004; 11:853–61.
42. Kashino G, Kondoh T, Nariyama N, Umetani K, Ohigashi T, Shinohara K, et al. Induction of DNA double-strand breaks and cellular migration through bystander effects in cells irradiated with the slit-type microplanar beam of the spring-8 synchrotron. Int J Radiat Oncol Biol Phys 2009; 74:229–36.
43. Ibahim MJ, Crosbie JC, Yang Y, Zaitseva M, Stevenson AW, Rogers PA, et al. An evaluation of dose equivalence between synchrotron microbeam radiation therapy and conventional broad-beam radiation using clonogenic and cell impedance assays. PLoS One 2014; 9:e100547.
44. Sprung CN, Cholewa M, Usami N, Kobayashi K, Crosbie JC. DNA damage and repair kinetics after microbeam radiation therapy emulation in living cells using monoenergetic synchrotron X-ray microbeams. J Synchrotron Radiat 2011; 18 (Pt 4):630–6.
45. Stupp R, Mason WP, van den Bent MJ, Weller M, Fisher B, Taphoorn MJ, et al. Radiotherapy plus concomitant and adjuvant temozolomide for glioblastoma. N Engl J Med 2005; 352:987–96.